Research Square

Preprints are preliminary reports that have not undergone peer review.
They should not be considered conclusive, used to inform clinical practice,
or referenced by the media as validated information.

Preparation of a high specificity imidacloprid monoclonal antibody and its application in homogeneous fluorescence immunoassay based on hydrogel beads assembling CdSe/ZnS quantum dots

Zixin Jin
Tianjin University of Science and Technology
Minghui Guo
Tianjin University of Science and Technology
Zhiwei Liu
Tianjin University of Science and Technology
Yuqing Yang
Tianjin University of Science and Technology
Meiyi Sun
Tianjin University of Science and Technology
Ziwuzhen Wang
Tianjin University of Science and Technology
Hongyu Shi
Tianjin University of Science and Technology
Shuo Wang
Nankai University
Wei Sheng
shengweijunchen@163.com
Tianjin University of Science and Technology

Research Article

Keywords: Imidacloprid, monoclonal antibody, fluorescent hydrogel beads, homogeneous fluorescence immunoassay, fruits and vegetables

Posted Date: November 2nd, 2026

DOI: https://doi.org/10.21203/rs.3.rs-11238045/v1

License: This work is licensed under a Creative Commons Attribution 4.0 International License.
Read Full License

Additional Declarations: No competing interests reported.

Abstract

The risk associated with imidacloprid (IMI) residues necessitates the development of highly sensitive detection methods for ensuring food safety. In this study, IMI-hapten is synthesized via the reaction of IMI with β-mercaptopropionic acid, and used to prepare immunogen, coating antigen, and IMI monoclonal antibody (IMI-mAb). An indirect competitive enzyme-linked immunosorbent assay (ic-ELISA) is established, yielding a half-maximal inhibitory concentration (IC_{50}) of 0.34 μg L^{-1} and a limit of detection (LOD) of 0.04 μg L^{-1}. To further enhance sensitivity and analytical efficiency, fluorescent hydrogel beads are engineered by embedding CdSe/ZnS quantum dots (QDs) into biocompatible chitosan hydrogel matrices. A homogeneous fluorescence immunoassay is subsequently established, relying on the competitive interaction between an antigen-conjugated quenching probe (AgNPs@IMI-OVA) and an antibody-labeled signal probe, which modulates the fluorescence intensity accordingly. Compared with conventional ELISA, this assay exhibits remarkable superiority, which achieves a LOD of 5.62×10^{-4} μg L^{-1} (representing over a 70-fold enhancement), eliminates tedious washing steps, and completes the entire assay within 20 min. Validation using spiked fruit and vegetable samples confirms the method's high specificity and reliability, demonstrating its great potential for the rapid screening of IMI residues in agro-products.

Introduction

Neonicotinoids represent a class of neuroactive insecticides derived from the molecular structure of nicotine. Developed in the early 1970 s, these synthetic analogues emerged from systematic structural optimization of nicotine, primarily targeting the enhancement of insecticidal potency and selectivity [1–2]. Imidacloprid (IMI) stands as one of the most extensively utilized neonicotinoid insecticides worldwide [3–4]. Since its commercial introduction in 1991, IMI has been deployed for pest management across more than 140 agricultural crops [5]. However, owing to its chemical stability and recalcitrance to biodegradation, IMI tends to accumulate in agricultural products and infiltrate aquatic environments following long-term application. Consequently, human exposure to IMI residues may trigger oxidative stress, induce DNA damage, and cause neurotoxicity, thereby posing significant threats to public health [6]. In response to these concerns, France and the European Union have implemented bans on the use or authorization of thiacloprid, while Canada has initiated phased withdrawal plans for IMI applications in agriculture [7]. Similarly, China's National Standard GB 2763 – 2021 [8] sets the Maximum Residue Limits (MRLs) for IMI in fruits and vegetables at 0.05-10 mg kg^{-1}, alongside an Acceptable Daily Intake (ADI) of 0.06 mg kg^{-1} bw. Furthermore, the European Food Safety Authority (EFSA) has established specific limit standards tailored to different crops [9]. Consequently, there is an urgent need to develop a sensitive and rapid detection method for IMI residues to ensure food safety and mitigate environmental risks.

Currently, various analytical methodologies have been developed for IMI detection, which are broadly categorized into instrumental analysis and immunoassay techniques. Among these, instrumental approaches predominantly rely on chromatographic and mass spectrometric techniques, including gas

chromatography-mass spectrometry (GC-MS) [10–11], high-performance liquid chromatography (HPLC) [12–13], HPLC-mass spectrometry (HPLC-MS) [14], ultra-performance liquid chromatography (UPLC) [15], and UPLC-tandem mass spectrometry (UPLC-MS/MS) [16], etc. Although these techniques offer high accuracy and reproducibility for trace residue quantification, they are often constrained by complex sample pretreatment protocols, prohibitive instrument costs, and the necessity for skilled operators [17–19]. In contrast, immunoassay techniques-such as enzyme-linked immunosorbent assay (ELISA), immunochromatography, and fluorescence immunoassay-rely on the specific recognition between antigens and antibodies [20–26]. Owing to their operational simplicity, low cost, and high sensitivity, these methods have emerged as a pivotal strategy for on-site monitoring of pesticide residues [27]. Nevertheless, conventional immunoassays still face challenges regarding detection sensitivity and practical applicability, necessitating further optimization.

Hydrogels are three-dimensional polymeric networks characterized by high hydrophilicity and porosity, capable of absorbing substantial amounts of water or biological fluids [28–29]. These materials exhibit exceptional biocompatibility and structural tunability, rendering them ideal candidates for advanced sensing platforms. Notably, hydrogels address critical bottlenecks in detection processes, such as analyte enrichment and selective recognition, thereby facilitating the development of high-performance analytical techniques [30–35]. Chitosan, a naturally derived polysaccharide, is increasingly favored in hydrogel fabrication owing to its inherent biodegradability, antibacterial activity, and the presence of abundant reactive amino and hydroxyl groups. These functional groups readily facilitate physical or chemical cross-linking, resulting in hydrogels with high porosity, strong adsorption capacity, and stimuli-responsive behavior (e.g., to pH and temperature). Consequently, chitosan-based hydrogels serve as versatile, cost-effective substrates for constructing sensitive and robust biosensing platforms [36].

- This study aims to develop a high-sensitivity, high-specificity, and field-applicable detection technique by focusing on the generation of specific antibodies and the construction of a novel immunoassay. Monoclonal antibody (mAb) are produced via standard hybridoma technology, involving murine immunization, cell fusion, and clone screening. Subsequently, an indirect competitive ELISA (ic-ELISA) is established and optimized based on these antibodies. To further elevate detection performance, fluorescent hydrogel beads are engineered to conjugate with mAbs, serving as signal probes, while silver nanoparticles (AgNPs) are functionalized with coating antigens to act as quenching probes. A homogeneous fluorescence immunoassay is thus developed, leveraging the competitive reaction between the two probes where the change in fluorescence intensity correlates with imidacloprid concentration. By capitalizing on the signal amplification capability of the hydrogel matrix and the efficient quenching efficiency of AgNPs, this method significantly enhances detection sensitivity and analytical throughput. This approach provides a robust solution for the rapid and precise quantification of IMI residues, offering significant practical implications for safeguarding food safety and ecological security.

Experimental

Materials and apparatus

Technical-grade imidacloprid was obtained from Tianjin Xien Biochemical Technology Co., Ltd. (Tianjin, China). IMI standard (purity ≥ 98%), acetamiprid standard (ACE, purity ≥ 98%), thiamethoxam standard (TMX, purity ≥ 98%), imidaclothiz standard (IMT, purity ≥ 98%), nitenpyram standard (NIT, purity ≥ 99%), thiacloprid standard (THI, purity ≥ 99%) were purchased from Yuanye Biotechnology Co., Ltd. (Shanghai, China). Ethyl-3-[3-(dimethylamino)propyl] carbodiimide (EDC), N-hydroxysuccinimide (NHS), ovalbumin (OVA), Freund's complete adjuvant (FCA), Freund's incomplete adjuvant (FIA), 3,3',5,5'-tetramethylbenzidine (TMB), hypoxanthine aminopterin thymidine (HAT), hypoxanthine thymidine (HT), 50% of polyethylene glycol (PEG, 1500), polyethyleneimine (PEI), and β-mercapto propionic acid were obtained from Sigma-Aldrich Co. Ltd. (St. Louis, MO, USA). Bovine serum albumin (BSA) was purchased from BioFroxx Co., Ltd. (Berlin, Germany). The BCA protein assay kit, and dimethyl sulfoxide (DMSO, cell culture grade) are obtained from Solarbio Science and Technology Co., Ltd. (Beijing, China). Fetal bovine serum (Ausource) was purchased from Gibco (Grand Island, NY, USA). Inorganic salts and other reagents were obtained from Sinopharm Chemical Reagent Co., Ltd. (Shanghai, China).

Preparation of IMI-hapten

The synthesis of the IMI hapten was performed according to the method described by Guo et al. [37], with minor modifications. Briefly, 0.5 g of IMI was dissolved in 7 mL of DMSO, followed by the addition of 0.66 g of potassium hydroxide. The mixture was heated in an oil bath at 100°C under a nitrogen atmosphere until complete dissolution was achieved. Separately, 0.618 g of β-mercaptopropionic acid was dissolved in 3 mL of DMSO and subsequently introduced into the reaction system. The reaction was maintained at 100°C for 4 h. Upon completion, the mixture was cooled to room temperature and diluted with 15 mL of deionized water. The pH was adjusted to 3.0 using 6 mol L^{-1} hydrochloric acid. The acidic solution was extracted three times with 10 mL aliquots of dichloromethane. The combined organic phases were back-extracted three times with 10 mL portions of 1 mol L^{-1} sodium bicarbonate solution. The aqueous layers from the back-extraction were pooled and re-acidified to pH 3.0, followed by triple extraction with 10 mL of aliquots of ethyl acetate. The combined ethyl acetate extracts were washed with a minimal volume of distilled water, and the organic phase was dried over anhydrous sodium sulfate. Finally, the solvent was removed via rotary evaporation, and the crude product was recrystallized from a small volume of acetone to afford the desired IMI-hapten.

Preparation of immonogen and coating antigen

The IMI-hapten (10 mg) was accurately weighed and dissolved in 700 μL of DMF with the aid of sonication. For carboxyl activation, 17 mg of EDC and 10 mg of NHS were sequentially added to the hapten solution under stirring. The activation reaction was allowed to proceed at room temperature in the dark for 12 h. Subsequently, the mixture was centrifuged at 5000 rpm for 10 min, and the supernatant containing the activated ester was collected for immediate use. Separately, carrier proteins were

prepared by dissolving bovine serum albumin (BSA, 44 mg) and ovalbumin (OVA, 17 mg and 27 mg for different batches) in 3.5 mL and 5.5 mL of PBS (0.01 mol L^{-1}, pH 7.4), respectively. The activated hapten solution was then slowly added dropwise to the protein solutions under vigorous stirring in an ice bath. The coupling reactions were maintained at 4°C for 12 h. Following incubation, the crude conjugates were purified by exhaustive dialysis against PBS at 4°C for 72 h, with the dialysis buffer being refreshed every 12 h. The resulting immunogen (IMI-BSA) and coating antigens (IMI-OVA, with hapten-to-protein molar ratios of 80:1 and 50:1) were aliquoted, and their concentrations were quantified using a BCA protein assay kit. All conjugates were stored at -20°C pending further use.

Preparation of IMI monoclonal antibody (IMI-mAb)

The generation of mAbs involved the fusion of splenocytes from immunized mice with myeloma cells, followed by the screening of clones capable of secreting specific antibodies (Fig. 1). Female BALB/c mice were initially housed for one week to acclimate prior to immunization. The initial immunization was performed by intraperitoneal injection of 100 μg of IMI-BSA emulsified in FCA. Subsequent booster immunizations were administered every two weeks using the same immunogen emulsified in FIA. Blood samples were collected from the tail vein 7 days post-secondary immunization to monitor serum titers and inhibition rates via ic-ELISA. The mouse exhibiting the highest immune response was selected for splenocyte fusion. Splenocytes were fused with SP2/0 myeloma cells via PEG-mediated fusion. Hybridomas were screened using HAT medium. Following three rounds of subcloning by limiting dilution, a stable hybridoma cell line secreting IMI-specific mAbs was established. The mAbs were subsequently purified from the ascites for characterization. All animal procedures were approved by the Institutional Animal Care and Use Committee (IACUC) of Tianjin University of Science and Technology (Approval No. 2023050) and conducted in strict accordance with the guidelines.

Preparation of QDs@hydrogel beads

The synthesis method of hydrogel beads was borrowed from Li et al. [38] and slightly modified. First, 200 mg of chitosan was packed in a small brown bottle containing 5 mL of ultra-pure water and ultrasounded until dissolved. Then, 100μL glacial acetic acid was quickly added to the solution and stirred at room temperature for 40 min. After 50 μL of CdSe/ZnS QDs was added, the sol was obtained by stirring at room temperature for 10 h. The hydrogel is drawn, and, using a 5 mL syringe, it is slowly dropped into a solution of sodium citrate (0.1 mol L^{-1}) containing 4 g of sodium hydroxide. The drip process should be applied evenly so that the hydrogel beads are the same size. After soaking for 10 h, the hydrogel was filtered, vacuum-dried and collected, and stored at 4°C.

Preparation of signal probes

The fluorescent hydrogel beads were first functionalized by soaking in a pH 7.4 PBS solution containing PEI for 3 h. Subsequently, the microbeads were transferred using polyethylene forceps into 200 μL

reaction mixtures containing 25, 30, 35, 40 and 45 μg of the IMI-mAb respectively, as well as 0, 2, 4, and 6 μL of potassium carbonate. The conjugation reaction was allowed to proceed at 37°C for 3 h to yield the QDs@hydrogel@mAb signal probes. Following this, the probes were immersed in a 2 mL solution of 0.2% (w/v) BSA and incubated at 37°C for 1 h to block any remaining nonspecific binding sites. Finally, the resulting signal probes were washed three times with PBS, lyophilized or air-dried, and stored in amber centrifuge tubes at 4°C pending use.

Preparation of AgNPs

The synthesis of AgNPs was adapted from Hu et al. [39] with slight modifications. Briefly, 4 mL of $AgNO_3$ stock solution (7×10^{-2} mol L^{-1}), 80 mL of ultrapure water, and 6 mL of sodium citrate solution (1.7×10^{-2}mol L^{-1}) were added sequentially to a conical flask. The mixture was stirred for 10 min to ensure homogeneity. Subsequently, 4 mL of $NaBH_4$ solution (3×10^{-3} mol L^{-1}) was rapidly injected into the reaction system under vigorous stirring. The reduction reaction was allowed to proceed for 30 min, after which the resulting AgNPs colloid was stored in an amber bottle at 4°C.

Preparation of quenching probes (AgNPs@IMI-OVA)

The AgNPs@IMI-OVA quenching probes were synthesized via a facile electrostatic assembly strategy. Briefly, 1 mL of AgNPs was mixed with 10, 20, 30, 40 and 50 μg of IMI-OVA conjugate, and 0, 2, 4, and 6 μL of K_2CO_3 (0.2 mol L^{-1}) in a 1.5 mL centrifuge tube. The coupling reaction was allowed to proceed at 4°C for 1 h to facilitate the adsorption of OVA onto the negatively charged AgNPs surface. Subsequently, 10 μL of 1 mol L^{-1} NaCl was introduced to stabilize the colloidal system, followed by the addition of 10 μL of BSA (1 mg mL^{-1}) to block any remaining nonspecific binding sites; the reaction was continued for another hour. Finally, the AgNPs@IMI-OVA conjugates were purified by centrifugation at 10,000 rpm for 30 min at 4°C. The supernatant was discarded, and the pellet was resuspended in 300 μL of PBS (pH 7.4) and stored at 4°C pending further use.

Principle and procedure of homogeneous fluorescence immunoassay

In this study, as shown in Fig. 2, a homogeneous fluorescence immunoassay is developed based on a competitive reaction between IMI and a quenching probe for binding sites on a signal probe. As shown in Fig. 2A, red-emitting CdSe/ZnS quantum dots (QDs, λem = 619 nm) are encapsulated within chitosan-based hydrogel beads modified with PEI, which imparts a surface charge to the matrix. The resulting QDs@hydrogel beads are conjugated with monoclonal antibodies (mAb) to construct the signal probe (QDs@hydrogel beads@mAb). Concurrently, As shown in Fig. 2B, silver nanoparticles (AgNPs) coated with IMI-OVA are synthesized as the quenching probe (AgNPs@IMI-OVA), leveraging the efficient fluorescence quenching capability of AgNPs.

Under optimized experimental conditions, the analytical procedure is conducted as follows : 1 mL of IMI standard solution (concentrations ranging from 0 to 50 μg L^{-1}) is mixed with the QDs@hydrogel@mAb signal probe, followed by the addition of 20 μL of the AgNPs@IMI-OVA quenching probe. After thorough mixing and incubation at room temperature for 20 min, the fluorescence intensity is measured using a spectrofluorometer. A calibration curve is established by plotting the fluorescence intensity against the logarithm of IMI concentration based on triplicate measurements. The limit of detection (LOD) is calculated as 3σ/S, where σ represents the standard deviation of blank signals (n ≥ 3) and S denotes the slope of the calibration curve.

As shown in Fig. 2C, the detection mechanism relies on the specific antigen–antibody interaction. In the absence of free IMI in the sample, the mAb on the signal probe preferentially binds to the IMI-OVA immobilized on the AgNPs surface. This proximity facilitates the quenching of QDs fluorescence by AgNPs, resulting in minimal fluorescence intensity. Conversely, when target IMI is present, it competitively inhibits the binding between the signal probe and the quenching probe. As the concentration of IMI increases, fewer signal probes are captured by the quenching probes; consequently, the quenching efficiency decreases and the fluorescence intensity of the system increases proportionally.

Sample treatment

The feasibility of the developed method was validated using locally sourced apples, tomatoes, and cucumbers. Sample pretreatment was slightly modified based on the method reported by Xu et al [40]. Briefly, 10 g of homogenized sample was weighed and spiked with IMI at concentrations of 50, 100, and 200 μg kg^{-1}. The spiked samples were extracted with 20 mL of a methanol water solution (7:3, *v/v*) under oscillatory shaking at room temperature for 10 min. Following filtration, the filtrate was concentrated by rotary evaporation, and the residue was reconstituted in 10 mL of phosphate buffer (PB, 10 mM, pH 7.4) prior to fluorescence immunoassay. The accuracy of the method was further confirmed by HPLC, and the detailed sample preparation procedures and instrumental parameters for HPLC are provided in Supplementary Materials (Table S1, Parameters of liquid phase instruments).

Results and discussion

Characterization of IMI-hapten and complete antigen

This work describes the synthesis of the IMI-hapten via nucleophilic substitution of the chlorine atom on the pyridine ring of IMI with β-mercapto propionic acid, yielding a product with a theoretical molecular weight of 325 Da. To verify successful conjugation, the product is characterized by mass spectrometry under sodium adduct mode (Fig. 3A). As depicted in the spectrum, the observed peak at m/z348 corresponds to the sodium adduct ($[M + Na]^+$, 348), confirming the expected molecular mass. Additionally, an extra peak at m/z673 is attributed to the hapten dimer ($[2M + Na]^+$, 673), which is likely formed due to the relatively high analyte concentration under the ionization conditions. Collectively,

these mass spectrometric results confirm the successful synthesis of the IMI-hapten with high purity, rendering it suitable for subsequent preparation of coating antigen and immunogen.

The successful conjugation of IMI to BSA and OVA-yielding IMI-BSA and IMI-OVA, respectively, and which is further confirmed by UV-Vis absorption spectroscopy (Fig. 3B). Following coupling via the activated ester method, distinct shifts in the maximum absorption wavelengths are observed. The IMI-hapten exhibits a peak at 266 nm, while IMI-BSA and IMI-OVA display red-shifted maxima at 276 nm and 278 nm, respectively. These spectral changes are consistent with the formation of stable hapten–carrier conjugates, as the protein matrix induces microenvironmental alterations that affect the electronic structure of the conjugated IMI moiety. The observed bathochromic shifts corroborate the successful preparation of both IMI-BSA and IMI-OVA, validating their suitability for subsequent immunoassay development.

Characterization of IMI monoclonal antibody (IMI-mAb)

Mice are immunized four times, and the specific immunological responses are summarized in Table S2 (Antiserum data after the fourth immunization). Following the fourth immunization, antiserum titers are determined via indirect ELISA. Among them, mouse No. 1 exhibits a titer of 1:4000, mice Nos. 2 and 6 reach 1:8000, and mice Nos. 3, 4, and 5 show titers of 1:6000. Although mouse No. 1 displays a relatively lower titer compared to others, its antiserum achieves a favorable inhibition rate of 31% (OD_{450} = 0.96 at 1:4000 dilution), indicating high functional affinity. Based on this optimal balance of titer and inhibitory activity, mouse No. 1 is selected for booster immunization and subsequent hybridoma cell fusion experiments. Three rounds of limiting dilution cloning yields a stable hybridoma cell line (2C1-1G10-F9-B7) secreting the desired antibodies. These cells are injected into mice for ascites production, and the antibodies are subsequently purified.

Establishment of indirect competitive enzyme-linked immunosorbent assay (ic-ELISA)

The optimum working concentrations for coating antigen dosage, coating reagent volume, and antibody dilution ratio are determined via checkerboard titration (Fig. 3C and 3D). To ensure detection accuracy, only combinations yielding an OD_{450} value between 0.8 and 1.2 and exhibiting high sensitivity toward IMI are selected. Among the eight parameter combinations screened, inhibition rates are measured and standard curves are independently plotted for each. The IC_{50} and IC_{15} values are calculated accordingly. Comparative analysis reveals that the combination of a 50:1 coating ratio (0.05 μg/well) and an antibody dilution of 32,000 yields the lowest IC_{50} (0.36 ± 0.03 μg L^{-1}) and IC_{15} (0.04 ± 0.02 μg L^{-1}) across all tested conditions. This optimal condition is therefore adopted for subsequent ic-ELISA validation and immunoassay development. Subsequently, a standard curve is established under the optimized conditions described above (Fig. 3E). From this curve, the IC_{50} of the ELISA is determined to be 0.34 μg L^{-1}, the IC_{15} is 0.04 μg L^{-1}, and the linear dynamic range spans 0.07–1.45 μg L^{-1}. These parameters confirm

that the monoclonal antibody developed in this study exhibits high sensitivity and suitable analytical performance for IMI quantification.

To evaluate the specificity of the IMI-mAb, five neonicotinoid structural analogues are subjected to ELISA analysis using the same protocol. Standard curves are generated for each compound, and their IC_{50} values are calculated to determine cross-reactivity rates (Fig. 3F). Notably, IMT demonstrates a moderate cross-reactivity (30%-40%), likely attributable to its structural similarity and shared functional groups with IMI. Results indicate that ACE shows negligible cross-reactivity (< 10%), which is considered insignificant for practical applications. The other three analogues exhibit no detectable cross-reactivity. This level of cross-reactivity is acceptable for selective detection of IMI.

Characterization and optimization of signal probe

The overall shape and surface features of the prepared hydrogel beads are investigated via scanning electron microscopy (SEM). As illustrated in Fig. 4A, the hydrogel beads exhibit a spheroidal morphology with a relatively uniform shape, and their diameter is approximately 1 mm. The surface appears relatively rough, which may facilitate the loading of functional materials. Figure 4B provides a high - magnification view of the hydrogel bead surface, clearly revealing the network structure and cross - linking state of the hydrogel. This porous and cross-linked structure endows the hydrogel with excellent potential as a carrier for QDs) as it can effectively encapsulate and stabilize the QDs. The signal probe (QDs@hydrogel beads@mAb) is excited by a suitable exciter, and the fluorescence is recorded using a dark-field camera. As shown in Fig. 4C, the stimulated signal probe emits strong red fluorescence. This indicates that the probe possesses good fluorescence performance, along with uniform shape and size, as well as favorable dispersion. The uniform fluorescence and morphology suggest that the QDs are successfully integrated into the hydrogel matrix and retain their optical properties, while the hydrogel matrix also ensures the stability and dispersibility of the QDs.

The fluorescent hydrogel beads are further characterized by X-ray photoelectron spectroscopy (XPS) to elucidate their elemental composition. As shown in Fig. 4D, the full-scan XPS spectrum of the hydrogel beads reveals distinct characteristic peaks corresponding to the elements Se 3d, S 2p, C 1s, N 1s, Cd 3d, O 1s, and Zn 2p. The identification of these elements confirms the successful incorporation of CdSe/ZnS QDs (which contain Cd, Se, Zn, and S) and the hydrogel matrix (which contains C, N, O, etc.) into the composite system. This elemental analysis provides direct evidence for the composition of the hydrogel-based signal probe. To gain more detailed insights into the chemical states of the elements, high-resolution XPS spectra (Fig. S1A-G) of Cd, Se, Zn, S, C, N, and O. Overall, the XPS analysis comprehensively validates the successful fabrication of the QD-doped hydrogel-based signal probe.

To achieve sufficient fluorescence signal and sensitivity, the addition amounts of IMI-mAb and K_2CO_3 are optimized during the preparation of the signal probe (QDs@hydrogel beads@mAb). As illustrated in Fig. 4E, the coupling amount of the fluorescent hydrogel beads with the IMI-mAb gradually increases as the supplemental amount of mAb rises. When the IMI-mAb addition amount reaches 35 μg or higher, the

coupling amount tends to stabilize, indicating that the coupling process reaches saturation at this point. In Fig. 4F, when the added volume of K_2CO_3 is 0 μL or 2 μL, the coupling amounts of the antibody and hydrogel beads are comparable, with the coupling amount at 2 μL being the highest. This suggests that a pH environment closer to the optimal range is achieved at 2 μL of K_2CO_3. Excessively alkaline conditions (e.g., volumes > 2 μL) appear to be unfavorable for the preparation of the signal probe, as the coupling amount decreases with further increases in K_2CO_3 volume. Therefore, the optimal addition volume of K_2CO_3 is determined to be 2 μL, and the optimal addition amount of the monoclonal antibody is 35 μg. These optimized parameters ensure a high coupling efficiency, which is critical for obtaining a signal probe with robust fluorescence performance and sensitivity.

Characterization and optimization of quenching probe

In this experiment, the morphology and size of the prepared silver nanoparticles (AgNPs) are observed via transmission electron microscopy (TEM). As shown in Fig. 5A, the AgNPs exhibit a small, approximately circular shape and are well dispersed, indicating a uniform particle size and favorable colloidal stability. The ultraviolet (UV) absorption spectra of the AgNPs and the AgNPs@IMI-OVA quenching probe are recorded using a UV-spectrophotometer. As illustrated in Fig. 5B, the UV absorption peak of the pristine AgNPs is located at 390 nm. After being encapsulated with IMI-OVA, the maximum absorption peak of the probe is significantly redshifted to 400 nm. This redshift in the absorption peak is a typical phenomenon associated with the interaction between the AgNPs and the biomolecule (IMI-OVA), which verifies that the AgNPs@IMI-OVA quenching probe has been successfully prepared. The successful preparation of this probe lays a foundation for subsequent applications (such as sensing or bioimaging) that rely on the optical properties of the AgNPs-biomolecule complex.

To achieve the optimal quenching effect of the AgNPs@IMI-OVA quenching probe, the amounts of coating antigen (IMI-OVA) and K_2CO_3 incorporated during synthesis are systematically investigated. As demonstrated in Fig. 5C, when the amount of coating antigen exceeds 30 μg, the absorbance of AgNPs@IMI-OVA stabilizes (no further decrease), indicating that the coupling of the coating antigen to AgNPs has reached saturation. This suggests that 30 μg represents the maximum effective loading capacity of IMI-OVA onto the AgNPs under the experimental conditions. In Fig. 5D, the addition of 2 μL of K_2CO_3 results in the lowest absorbance of the system, which corresponds to the highest binding efficiency between AgNPs and the coating antigen. This is attributed to the fact that the pH of the quenched probe preparation system is most favorable for the coupling reaction at this K_2CO_3 volume (excessively alkaline or acidic environments would compromise coupling efficiency). Thus, the optimal amount of coating antigen is determined to be 30 μg, and the optimal volume of potassium carbonate is 2 μL. These optimized parameters ensure the highest quenching efficiency of the AgNPs@IMI-OVA probe, which is essential for its subsequent application in sensitive detection scenarios.

Working parameters optimization of fluorescence immunoassay

In the homogeneous immune-competitive reaction system, to ensure that the signal probes not bound to the target are fully quenched, the addition amount of the quenching probe and the reaction time are optimized. As shown in Fig. 6A, when the addition amount of the quenching probe exceeds 20 μL, the fluorescence intensity of the system hardly decreases, indicating that the signal probes have been quenched to the maximum extent at this time. As shown in Fig. 6B, when the reaction time is less than 20 min, the signal probes in the system do not fully combine with IMI. Therefore, for the IMI fluorescence immunoassay based on QDs@hydrogel beads, the optimal addition amount of the quenched probe and the optimal reaction time are 20 μL and 20 min, respectively.

Sensitivity analysis

Under the optimized detection conditions, the sensitivity of the homogeneous fluorescence immunoassay based on AgNPs quenching QDs@hydrogel beads is systematically evaluated. As shown in Fig. 6C, standard solutions of IMI at varying concentrations are analyzed, and the limit of detection (LOD) is calculated based on a signal-to-noise ratio of 3δ. The results reveal that the proposed method achieves an ultralow LOD of 5.62×10^{-4} μg L^{-1}, along with a broad linear dynamic range spanning from 0.01 to 100 μg L^{-1} (R^2 = 0.991). Such a favorable linear relationship indicates excellent signal response and accuracy across a wide concentration span. These findings confirm that the assay possesses high sensitivity and is highly suitable for the trace-level detection of IMI in complex samples.

Specific analysis

Subsequently, the specificity of the proposed method is evaluated by selecting five neonicotinoid pesticide structural analogues of IMI (namely ACE, IMT, THI, NIT, and TMX-as interfering substances). As shown in Fig. 6D, the fluorescence responses of these analogues are compared with that of IMI. The results indicate that, except for IMT (which exhibits a relatively weak yet distinguishable response), the other analogues show no obvious fluorescence change in the reaction system. This demonstrates that the QDs@hydrogel beads-based fluorescence immunoassay for IMI possesses excellent specificity, effectively discriminating IMI from its structural analogues. Consequently, this method is highly suitable for practical applications.

Samples analysis

To evaluate the accuracy of the proposed method, recovery experiments are conducted using three representative food samples (tomato, cucumber, and apple-subjected to gradient dilution), followed by immune competitive reaction and HPLC analysis. As presented in Table 1, the recovery rates obtained by the fluorescence immunoassay range from 84.34% to 109.43%, while those determined by HPLC fall between 86.64% and 106.46%. Notably, the recovery profiles of both methods exhibit consistent trends across all spiked concentrations and sample types. These results confirm that the developed immunoassay possesses reliable accuracy and is comparable to the conventional HPLC, thereby validating its suitability for quantitative determination of IMI in real food matrices.

Table 1
Determination of food samples (n = 3).

Sample	Added concentration	Fluorescence immunoassary		HPLC	
	(μg kg^{-1})	Recovery rate (%)	CV (%)	Recovery rate (%)	CV (%)
Tomato	50	95.34 ± 3.64	3.82	94.16 ± 7.11	7.55
	100	87.32 ± 6.23	7.13	97.47 ± 1.01	1.04
	200	105.34 ± 7.21	6.84	86.64 ± 1.74	2.00
Cucumber	50	104.11 ± 4.24	4.07	98.97 ± 1.40	1.41
	100	109.43 ± 1.87	1.71	93.09 ± 2.84	3.05
	200	88.34 ± 8.23	9.32	94.02 ± 2.70	2.82
Apple	50	90.89 ± 5.09	5.60	106.46 ± 1.58	1.48
	100	100.31 ± 3.04	2.97	103.59 ± 6.98	6.73
	200	84.34 ± 6.57	8.17	93.79 ± 0.95	1.01

Analytical performance of homogeneous immunoassay

The homogeneous fluorescence immunoassay developed in this study is systematically compared with previously reported methods for IMI determination (Table S3, An overview on the reported assays for determination of IMI). As summarized in the table, the proposed method achieves a LOD of 5.62×10^{-4} μg L^{-1}, which is significantly lower than most existing techniques-including terahertz metamaterial sensors (0.072 mg kg^{-1}), aptamer-based fluorescence sensing (52.42 ng mL^{-1}), inverse opal photonic crystal hydrogel strips (0.065 μg mL^{-1}), red-emitting Eu-IMDC probe platforms (75 nM), and SERS-based Ag/AuNPs-TiO_2-OCC (4.1×10^{-6} μg/mL). Although the SERS method exhibits a slightly lower LOD, it lacks portability and requires complex instrumentation. These results highlight the superior performance of the proposed method for trace-level IMI detection in complex matrices, positioning it as a robust alternative to conventional HPLC and emerging nanomaterial-based sensors.

Conclusions

This study presents significant advances in the sensitive and rapid detection of IMI, a representative neonicotinoid insecticide. An indirect competitive ELISA is first established using a high-affinity monoclonal antibody, exhibiting an IC_{50} of 0.34 μg L^{-1}, a LOD of 0.04 μg L^{-1}, and a linear range of 0.07–1.45 μg L^{-1}. To further improve analytical performance, a homogeneous fluorescence immunoassay is developed by employing chitosan hydrogel as a novel carrier for quantum dot-based signal probes. Compared with ELISA, the proposed fluorescence platform achieves a substantially lower LOD of

5.62×10^{-4} μg L^{-1} and a markedly broader linear dynamic range spanning 0.01–100 μg L^{-1}, thereby enabling accurate quantification across diverse concentration levels. In practical applications, the fluorescence immunoassay demonstrates excellent accuracy, with recovery rates ranging from 84.34% to 109.43% in food matrices (tomato, cucumber, and apple), which closely align with those obtained by the standard HPLC method. The assay protocol is remarkably simple, requiring only 20 min without tedious washing or separation steps, thus minimizing operational complexity and human-induced errors. Future efforts will focus on refining the fluorescent signal probe to further extend the detection limits and dynamic range for ultra-trace analysis in complex matrices. Moreover, integrating this assay with portable detection devices holds considerable promise for on-site monitoring of IMI residues in agricultural products, thereby strengthening food safety assurance and environmental surveillance. Collectively, this work establishes a robust methodological foundation for next-generation IMI detection technologies with broad applicability in food safety and ecological risk assessment.

Declarations

Competing interests

The authors declare that they have no known competing financial interests or personal relationships that could have appeared to influence the work reported in this paper.

Funding

This work was supported by the National Natural Science Foundation of China (No. 32502335) and National Key R & D Program of China (Project No. 2024YFF1105701).

Author Contribution

Zixin Jin: Investigation, Data curation, Writing-original draft, Funding acquisition. Minghui Guo: Formal analysis. Zhiwei Liu: Formal analysis. Yuqing Yang: Formal analysis. Meiyi Sun: Validation. Ziwuzhen Wang: Formal analysis. Hongyu Shi: Formal analysis. Shuo Wang: Conceptualization. Wei Sheng: Conceptualization, Funding acquisition, Supervision. All authors reviewed the manuscript.

Generative AI and AI-assisted technologies During the preparation of this work, the authors did not use any generative AI or AI-assisted technologies in the writing, preparation, generation, modification, or enhancement of the manuscript, figures, or graphical abstract.

References

1. Jeschke P, Nauen R, Schindler M, Elbert A (2011) Overview of the Status and Global Strategy for Neonicotinoids. J Agric Food Chem 59(7):2897–2908. https://doi.org/10.1021/jf101303g

2. Motaung TE (2020) Chloronicotinyl insecticide imidacloprid: Agricultural relevance, pitfalls and emerging opportunities. Crop Prot 131:105097. https://doi.org/10.1016/j.cropro.2020.105097
3. Tan G, Zhao Y, Wang M, Chen X, Wang B, Li QX (2020) Ultrasensitive quantitation of imidacloprid in vegetables by colloidal gold and time-resolved fluorescent nanobead traced lateral flow immunoassays. Food Chem 311:126055. https://doi.org/10.1016/j.foodchem.2019.126055
4. Hu L, Zhang Y, Luo Q, Li T, Lai W (2025) Oriented antibody coupling enhances lateral flow immunoassay sensitivity for imidacloprid detection in vegetables and fruits. J Food Compos Anal 148:108548. https://doi.org/10.1016/j.jfca.2025.108548
5. Nauen R, Jeschke P, Copping L (2008) Focus: Neonicotinoid insecticides Editorial. Pest Manag Sci 64(11):1081–1081. https://doi.org/10.1002/ps.1659
6. Zhang D, Lu S (2022) Human exposure to neonicotinoids and the associated health risks: A review. Environ Int 163:107201. https://doi.org/10.1016/j.envint.2022.107201
7. Zaharia R, Trotuș E, Trașcă G, Georgescu E, Șapcaliu A, Fătu V, Petrișor C, Mincea C (2023) Impact of Seed Treatment with Imidacloprid, Clothianidin and Thiamethoxam on Soil, Plants, Bees and Hive Products, Agriculture, p. 830. https://doi.org/10.3390/agriculture13040830
8. Zheng K, Lin R, Liu X, Wu X, Chen R, Yang M Multiresidue Pesticide Analysis in Tea Using GC-MS/MS to Determine 12 Pesticide Residues (GB 2763 – 2021), Molecules, 2022, p. 8419. https://doi.org/10.3390/molecules27238419
9. European Food A, Safety (2014) Reasoned opinion on the setting of MRLs for imazapyr in genetically modified soya bean and other oilseeds and in lentils. EFSA J 12(6):3743. https://doi.org/10.2903/j.efsa.2014.3743
10. Lodevico RG, Li QX, DETERMINATION OF TOTAL IMIDACLOPRID, RESIDUES IN COFFEE BY GAS CHROMATOGRAPHY-MASS SPECTROMETRY (2002) Anal Lett 35(2):315–326. https://doi.org/10.1081/AL-120002532
11. Buchweitz JP, Viner TC, Lehner AF (2019) Qualitative identification of imidacloprid in postmortem animal tissue by gas chromatography-tandem mass spectrometry. Toxicol Mech Methods 29(7):511–517. https://doi.org/10.1080/15376516.2019.1616344
12. Alizadeh R, mashalavi B, Yeganeh Faal A, Seidi S (2021) Development of ultrasound assisted dispersive micro solid phase extraction based on CuO nanoplate-polyaniline composite as a new sorbent for insecticides analysis in wheat samples. Microchem J 168:106422. https://doi.org/10.1016/j.microc.2021.106422
13. Hrybova NY, Khyzhan OI, Maksin VI, Kavshun LO, Tankha OL (2019) Determination of Xenobiotic Imidacloprid Content in Surface Waters. J Water Chem Technol 41(5):313–317. https://doi.org/10.3103/S1063455X19050072
14. Campillo N, Viñas P, Férez-Melgarejo G, Hernández-Córdoba M (2013) Liquid Chromatography with Diode Array Detection and Tandem Mass Spectrometry for the Determination of Neonicotinoid Insecticides in Honey Samples Using Dispersive Liquid–Liquid Microextraction. J Agric Food Chem 61(20):4799–4805. https://doi.org/10.1021/jf400669b

15. Batouti ME, Al-Harby NF, Abdelwahab MS, Metwally RA (2026) UPLC profiling of matcha extract capping biosynthesized copper oxide nanoparticles and their antimicrobial and cytotoxic potentials. Sci Rep 16(1):16317. https://doi.org/10.1038/s41598-026-47252-9
16. Wen Q, Cai J, Yang M, Xu X-y, Wei B-p, Wu Q, Zhao D-g (2026) Development and Validation of a UPLC-MS/MS Method for the Determination of Apalutamide in Human Plasma and Its Application in a Bioequivalence Study. Biomed Chromatogr 40(4):e70400. https://doi.org/10.1002/bmc.70400
17. Shi X, Yang F, Liu H, Zhang M, Sun X, Guo Y (2021) Supersensitive Electrochemiluminescence Aptasensor for Malathion Residues Based on ATO@TiO_2 and AgNPs. Food Anal Methods 14(11):2288–2297. https://doi.org/10.1007/s12161-021-02066-5
18. Chu HW, Unnikrishnan B, Anand A, Lin YW, Huang CC (2020) Carbon quantum dots for the detection of antibiotics and pesticides. J Food Drug Anal 28(4):539–557. https://doi.org/10.38212/2224-6614.1269
19. Cao C, Guo W (2024) Carbon dots-based fluorescent probe for the detection of imidacloprid residue in leafy vegetables. Food Chem 435:137578. https://doi.org/10.1016/j.foodchem.2023.137578
20. Du M, Yang Q, Liu W, Ding Y, Chen H, Hua X, Wang M (2020) Development of immunoassays with high sensitivity for detecting imidacloprid in environment and agro-products using phage-borne peptides. Sci Total Environ 723:137909. https://doi.org/10.1016/j.scitotenv.2020.137909
21. Zhai R, Chen G, Liu G, Huang X, Xu X, Li L, Zhang Y, Xu D (2023) A.M. Abd El-Aty, Comparison of Chemiluminescence Enzyme Immunoassay (Cl-ELISA) with Colorimetric Enzyme Immunoassay (Co-ELISA) for Imidacloprid Detection in Vegetables, Foods, p. 196. https://doi.org/10.3390/foods12010196
22. Gross MS, Woodward EE, Hladik ML (2022) Evaluation of ELISA for the analysis of imidacloprid in biological matrices: Cross-reactivities, matrix interferences, and comparison to LC-MS/MS. 286:131746. https://doi.org/10.1016/j.chemosphere.2021.131746
23. Li K, Li QX (2000) Development of an Enzyme-Linked Immunosorbent Assay for the Insecticide Imidacloprid. J Agric Food Chem 48(8):3378–3382. https://doi.org/10.1021/jf991257n
24. Elbaz GA, Zaazaa HE, Monir HH, Abd El Halim LM, Atty SA (2022) Nano eco-friendly voltammetric determination of pesticide, imidacloprid and its residues in thyme and guava leaves. Sustainable Chem Pharm 29:100799. https://doi.org/10.1016/j.scp.2022.100799
25. Fang Q, Wang L, Cheng Q, Cai J, Wang Y, Yang M, Hua X, Liu F (2015) A bare-eye based one-step signal amplified semiquantitative immunochromatographic assay for the detection of imidacloprid in Chinese cabbage samples. Anal Chim Acta 881:82–89. https://doi.org/10.1016/j.aca.2015.04.047
26. Wu S, Liu L, Duan N, Li Q, Zhou Y, Wang Z (2018) Aptamer-Based Lateral Flow Test Strip for Rapid Detection of Zearalenone in Corn Samples. J Agric Food Chem 66(8):1949–1954. https://doi.org/10.1021/acs.jafc.7b05326
27. Wang J, Wang X, Yang Y, Zhou X, Dai Z, Hao P, Han G, Yao J, Yu X, Ye Z (2025) Dual-readout fluorescence ‘turn-on’ lateral flow immunoassay for sensitive detection of imidacloprid. Biosens

Bioelectron 279:117379. https://doi.org/10.1016/j.bios.2025.117379

28. Cheng W, Wu X, Zhang Y, Wu D, Meng L, Chen Y, Tang X (2022) Recent applications of hydrogels in food safety sensing: Role of hydrogels. Trends Food Sci Technol 129:244–257. https://doi.org/10.1016/j.tifs.2022.10.004
29. Mehta P, Sharma M, Devi M (2023) Hydrogels: An overview of its classifications, properties, and applications. J Mech Behav Biomed Mater 147:106145. https://doi.org/10.1016/j.jmbbm.2023.106145
30. Wang J, Yang Q, Zhang L, Liu M, Hu N, Zhang W, Zhu W, Wang R, Suo Y, Wang J (2018) A hybrid monolithic column based on layered double hydroxide-alginate hydrogel for selective solid phase extraction of lead ions in food and water samples. Food Chem 257:155–162. https://doi.org/10.1016/j.foodchem.2018.02.143
31. Li M, Li X, Xu M, Liu B, Yang M, Chen Z, Gao T, James TD, Wang L, Xiao H (2021) A ratiometric fluorescent hydrogel of controlled thickness prepared continuously using microtomy for the detection and removal of Hg(II). Chem Eng J 426:131296. https://doi.org/10.1016/j.cej.2021.131296
32. Luo Q, Ren T, Lei Z, Huang Y, Huang Y, Xu D, Wan C, Guo X, Wu Y (2022) Non-toxic chitosan-based hydrogel with strong adsorption and sensitive detection abilities for tetracycline. Chem Eng J 427:131738. https://doi.org/10.1016/j.cej.2021.131738
33. Tong X, Cai G, Zhu Y, Tong C, Wang F, Guo Y, Shi S (2022) Integrating smartphone-assisted ratiometric fluorescent sensors with in situ hydrogel extraction for visual detection of organophosphorus pesticides. New J Chem 46(17):8195–8202. https://doi.org/10.1039/d1nj05614j
34. Gao Y, Gao M, Chen G, Tian M, Zhai R, Huang X, Xu X, Liu G, Xu D (2021) Facile synthesis of covalent organic frameworks functionalized with graphene hydrogel for effectively extracting organophosphorus pesticides from vegetables. Food Chem 352:129187. https://doi.org/10.1016/j.foodchem.2021.129187
35. Yan X, Wang T, Li H, Zhang L, Xin H, Lu G (2022) Flexible Aggregation-Induced Emission-Active Hydrogel for On-Site Monitoring of Pesticide Degradation. ACS Nano 16(11):18421–18429. https://doi.org/10.1021/acsnano.2c06544
36. Basiglio B, Ribone SR, Cerutti JP, De Leger W, Longhi MR, Aiassa V, Smet M, Dehaen W, Zoppi A (2026) Synthesis of functionalized chitosan hydrogels for pH-responsive drug delivery. Int J Biol Macromol 355:151569. https://doi.org/10.1016/j.ijbiomac.2026.151569
37. Zhu G-n, Gui W-j, Zheng Z-t, Cheng J-l, Wu G (2006) Synthesis and Identification of Artificial Antigen for Imidacloprid. Agricultural Sci China 5(4):307–312. https://doi.org/10.1016/S1671-2927(06)60054-0
38. Li F, Zhao A, Li Z, Xi Y, Jiang J, He J, Wang J, Cui H (2022) Multifunctionalized Hydrogel Beads for Label-Free Chemiluminescence Imaging Immunoassay of Acute Myocardial Infarction Biomarkers. Anal Chem 94(5):2665–2675. https://doi.org/10.1021/acs.analchem.1c05434

39. Hu D, Yang X, Chen W, Feng Z, Hu C, Yan F, Chen X, Qu D, Chen Z (2021) Rhodiola rosea Rhizome Extract-Mediated Green Synthesis of Silver Nanoparticles and Evaluation of Their Potential Antioxidant and Catalytic Reduction Activities. ACS Omega 6(38):24450–24461. https://doi.org/10.1021/acsomega.1c02843
40. Xu T, Gong Xu Q, Li H, Wang J, Li QX, Shelver WL, Li J (2012) Strip-based immunoassay for the simultaneous detection of the neonicotinoid insecticides imidacloprid and thiamethoxam in agricultural products. Talanta 101:85–90. https://doi.org/10.1016/j.talanta.2012.08.047

Figures

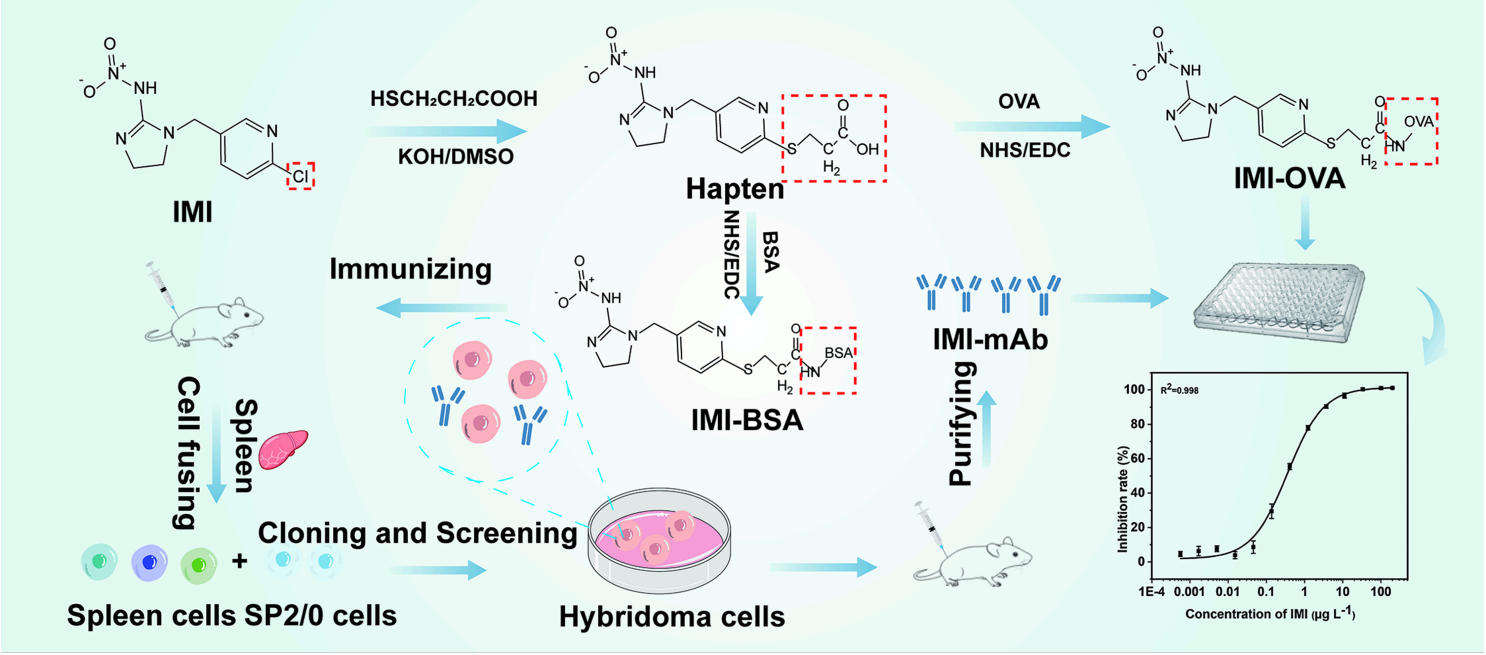


Figure 1

Schematic of hapten synthesis and preparation of IMI-mAb

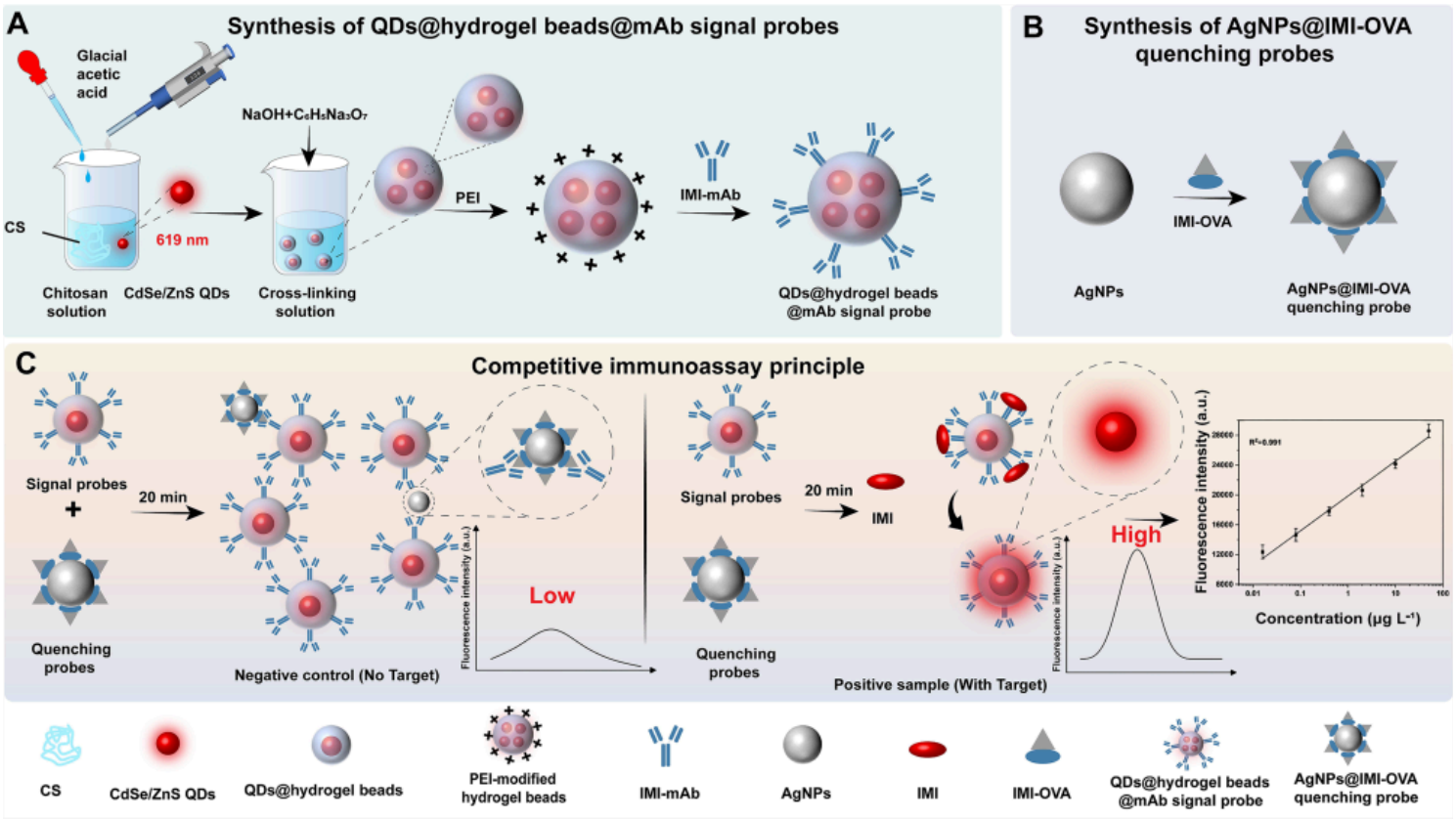


Figure 2

Schematic diagram of fluorescence immunoassay for detection IMI based on QDS@hydrogel beads. Synthesis of QDs@hydrogel beads@mAb signal probes (A), AgNPs@IMI-OVA quenching probes (B), competitive immunoassay principle (C).

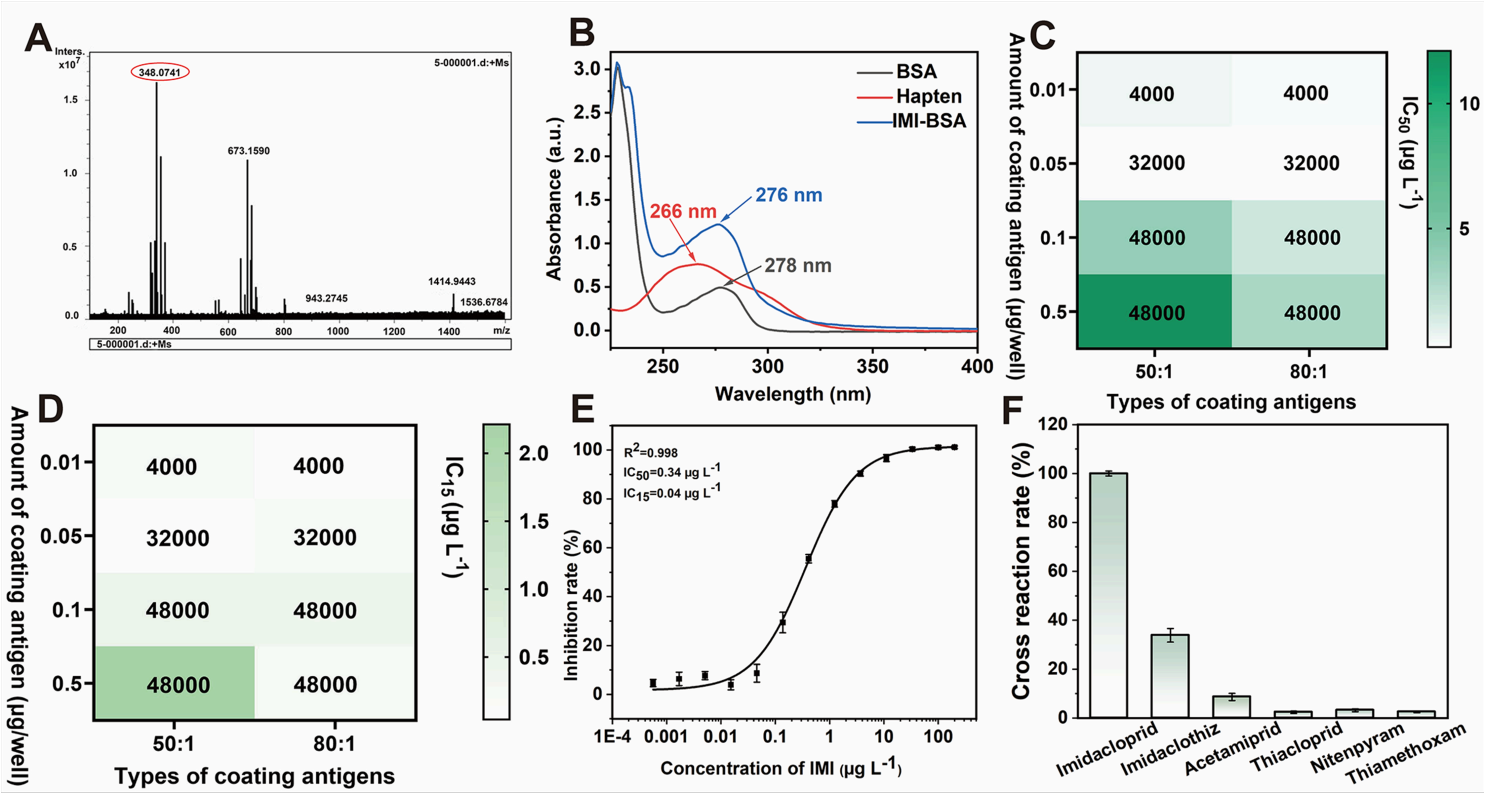


Figure 3

Mass spectrum of IMI-hapten (A), Ultraviolet-visible spectra of BSA, hapten and immunogen (B), optimization of ELISA conditions : coating concentration, coating antigen type, and antibody dilution (n=3) (C and D), standard competitive inhibition curve of the IMI ELISA (E), specificity analysis of IMI-mAb (F).

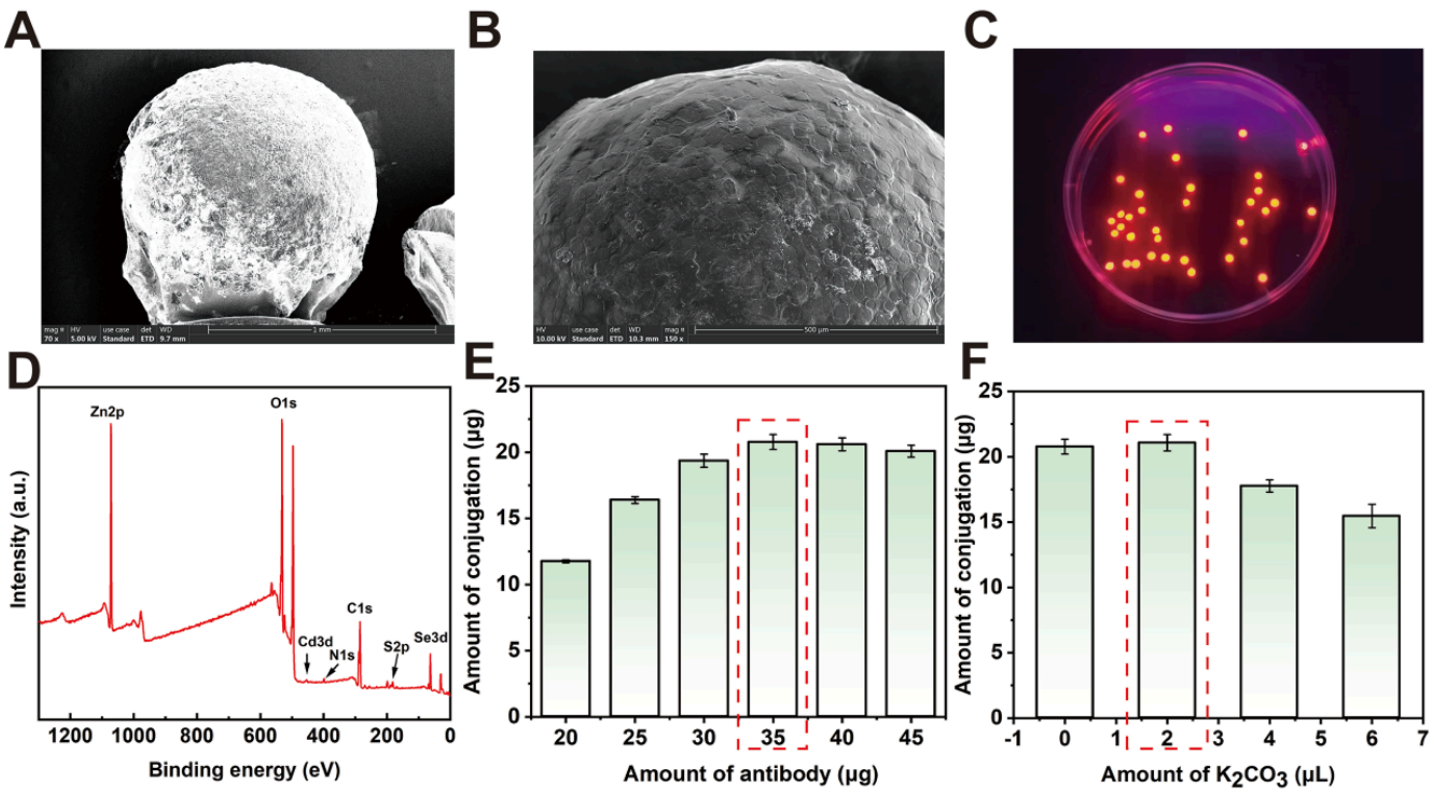


Figure 4

Characterization and optimization of QDs@hydrogel beads@mAb signal probes. SEM images of hydrogel beads at different magnification (A and B), fluorescence image of the QDs@hydrogel beads@mAb signal probe under UV excitation (C), XPS spectrum of fluorescence hydrogel beads (D), optimization of IMI-mAb addition during the preparation of signal probe (E), optimization of K_2CO_3 addition during the preparation of signal probe (F).

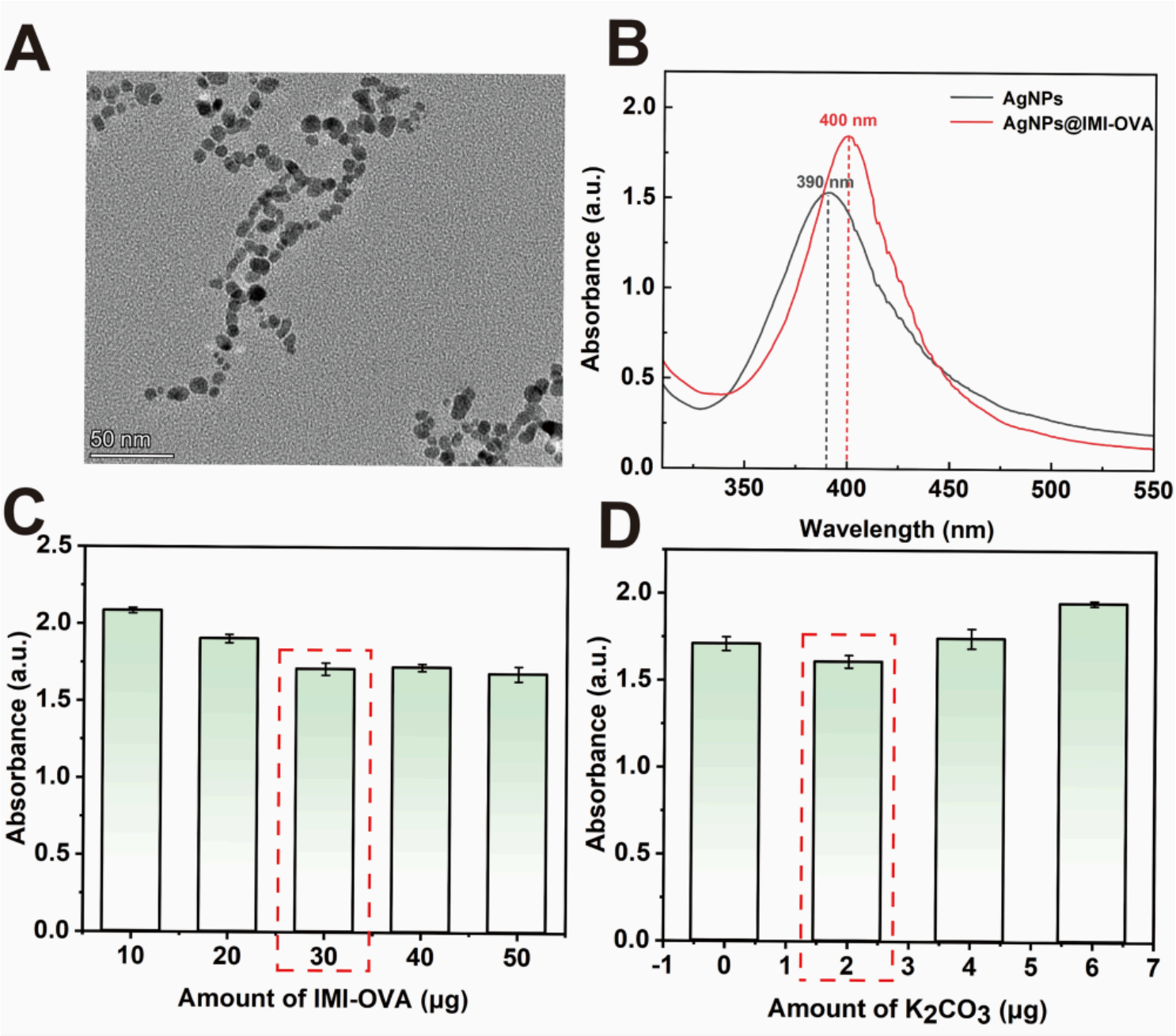


Figure 5

Characterization and optimization of AgNPs@IMI-OVA quenching probe. TEM images of AgNPs (A), Ultraviolet-visible spectra of AgNPs and IMI-OVA@AgNPs quenching probe (B), optimization of coating antigen addition during the preparation of quenchingprobe (C), optimal of during the preparation of quenching probe (D).

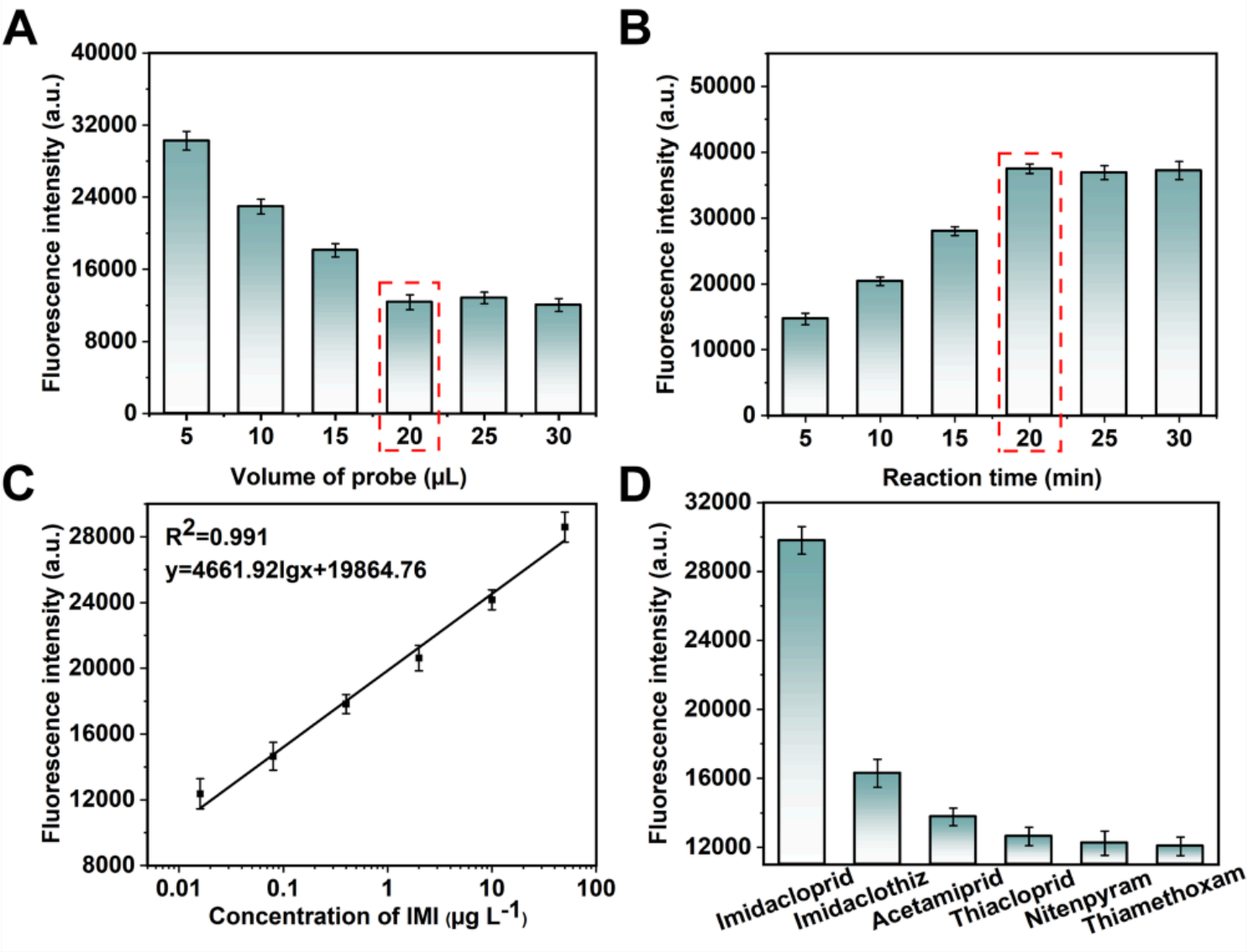


Figure 6

Optimization and performance evaluation of the fluorescence immunoassay. Optimization of quenching probe volume (A), optimization of reaction time (B), tandard competitive inhibition curve of the assay (C), specificity analysis of the assay (D).

Supplementary Files

This is a list of supplementary files associated with this preprint. Click to download.

- SupplymentaryMaterials.docx
- GA.tif